Derivation of the Shape of Raindrops

Brian Lim*
School of Applied and Engineering Physics, Cornell University
Ithaca, NY 14853
(Dated: May 19, 2006)

The solving for the shape of a raindrop, as reported by [1] is repeated in this project. Its governing equations are derived from basic equations, and the resulting solutions provided by numerical computations. The computer program procedure is also discussed. A comparison of the resulting model is done against the original paper [1] and with a photo of a raindrop from [2].

I. INTRODUCTION

To a layperson, a raindrop would have the shape of a tear drop, as often renditioned in popular media. However, to an acute individual, and as pointed out fervently by Fraser [17], a raindrop would have more of a spherical shape. The tear drop shape applies only just as the drop falls from a surface. It would then take a somewhat spherical form, and then distort to a shape like an oblate spheroid that many call a 'hamburger shape.' This is mainly because of the drag force on the falling drop causing it to be flattened. There are also other factors that give a raindrop its shape. Five key factors commonly agreed to affect the raindrop shape are

- surface tension
- hydrostatic pressure
- aerodynamic pressure
- internal circulation
- electric stress

Due to the scope of each factor and in keeping with the original work [1], the derivation in this paper neglects internal circulation and electric stress. There is another paper [3] that garnered a large number of citations prior to [1], and even though Beard and Chuang drew a lot from Pruppacher's work, they have refined the derivations and used slightly different techniques to arrive at a more accurate model. Much work has been done on calculating the shape of raindrops, and one may wonder why. A common application is so that the axis ratios and exact shape profiles of the drops can be determined to investigate how the drops would appear on weather satellites. By knowing the shapes, one can determine the intensity of rain and clouds from satellite images.

II. THEORY

A. Calculation of drop shape

The governing physical equation determining the drop shape is the Laplace-Young equation for pressure balance at the drop surface (see Eq (B9) for derivation)

$$\sigma\left(\frac{1}{R_1}+\frac{1}{R_2}\right)=\Delta p \tag{1}$$

where $\Delta p = p_i - p_e$ is the pressure difference across the interface, and R_1 and R_2 are the radii of curvature. Using the tangential coordinate system (see Appendix A 2), substituting Eqs (A2) and (A3), Eq (1) becomes

$$\sigma\left(\frac{d\phi}{ds}+\frac{\sin\phi}{x}\right)=p_i-p_e \tag{2}$$

Tangent angle coordinate system auxilliary equations:

$$\frac{dx}{ds} = \cos\phi \tag{3a}$$

$$\frac{dz}{ds} = \sin\phi \tag{3b}$$

By assuming the external pressure as, $p_e = 0$, and internal pressure as $p_i = (p_i)_t + \Delta\rho g z$, Bashforth and Adams (1883) were able to determine the shape of a sessile drop. $\Delta\rho = \rho_w - \rho_a$ is the density difference between the fluid inside the boundary and the fluid outside. Since the curvatures at the top of the drop are equal, i.e. $R_1 = R_2$, substituting the pressure expressions into Eq (1) gives $(p_i)_t = 2\sigma/R_t$, where R_t is the radius of curvature at the top. Eq (2) thus becomes

$$\sigma\left(\frac{d\phi}{ds}+\frac{\sin\phi}{x}\right)=\frac{2\sigma}{R_t}+\Delta\rho g z \tag{4}$$

The shape can be calculated by forward integration of $ds/d\phi$, from tangent angle 0 to 180^o, however, it is convenient to use the dimensionless form of Eq (4)

$$\sigma\frac{d\phi}{dS}=-\frac{\sin\phi}{X}+\frac{2}{C}+Z \tag{5}$$

where $dS = b ds$,$X = bx$, $C = bR_t$ and $Z = bz$, and inverse length $b = \sqrt{\Delta\rho g/\sigma}$.

B. Simple calculations using the new model

Aerodynamic pressure can be added to Eq. (2) to give

$$\sigma\left(\frac{d\phi}{ds}+\frac{\sin\phi}{x}\right)=(p_i)_t+\Delta\rho g z-p_a \tag{6}$$

*E-mail: bl223@cornell.edu

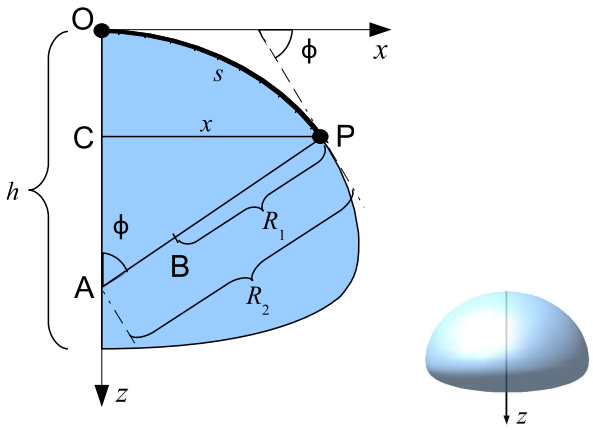

FIG. 1: Diagram of curve for the drop surface in the x-z plane with radius of curvature R_1 given by BP and R_2 by AP (both lying on the perpendicular to the curve at P). Adapted from Beard and Chuang [1]. At the side, a 3D revolvement of the drop.

At top, $p_i = (p_i)_t$ and $p_a = (p_a)_t$, so curvature $2\sigma/R_t = (p_i)_t - (p_a)_t$, and Eq. (6) becomes

$$\sigma d\phi = -\sigma \sin\phi/x + 2\sigma/R_t + \Delta\rho g z + (p_i)_t - (p_a)_t \quad (7)$$

with dimensionless form

$$\frac{d\phi}{dS} = -\frac{\sin\phi}{X} + \frac{2}{C} + Z + \frac{1}{\sigma b}[(p_a)_t - (p_a)] \quad (8)$$

Following [4], the aerodynamic pressure is based on measured distribution around sphere where $\theta = 0$ at the lower pole, so

$$p_a = \frac{1}{2}\rho U_0^2 \kappa(\theta) \quad (9)$$

where $\kappa(\theta)$ is the dimensionless pressure distribution. The $\kappa(\theta)$ distribution is obtained from a cubic spline interpolation of data from experiments by Fage [5].

Since $(p_a)_t = (1/2)\rho_a U_0^2 \kappa_t$ and $\kappa_t = \kappa(\pi)$, Eq (5) becomes

$$\frac{d\phi}{dS} = -\frac{\sin\phi}{X} + \frac{2}{C} + Z - \frac{We}{Q}[\kappa(\theta) - \kappa(\pi)] \quad (10)$$

where $We = a\rho U_0^2/2\sigma$ is the Weber number, $Q = bq$ is the dimensionless drop radius, q is the radius of an equivalent volumn sphere

Eq (10) can be solved by forward integration from the upper to lower poles, using the initial condition that its initial curvature is $d\phi/dS = 1/C$ (since $Z = 0$, $\kappa(\theta) = \kappa(\pi)$, and $d\phi/dS = \sin\phi/X$), and the boundary condition that the curve must be closed. This latter condition should be satisfied when the pressure support equals the weight of the drop.

C. Raindrop shape using p_a for a

At a given Reynolds number,

$$Re = \frac{\rho_a U_0 d}{\mu_a}, \quad (11)$$

the pressure drag can be calculated from the following integral of the pressure drag coefficient [1, 5]

$$C_{dp} = \int_{\theta=0}^{\theta=\pi} \frac{p - p_0}{\frac{1}{2}\rho U_0^2} d(\sin^2\theta)$$
$$= 2\int_0^{\pi} \kappa(\theta)\cos\theta\sin\theta d\theta \quad (12a)$$

and substituted into the drag equation from [6]

$$D = \frac{1}{2} C_d \rho_a U^2 A \quad (13)$$

To calculate the pressure drag at other Reynolds numbers, it is convenient to use an empirically defined analytical formula. Achenbach [7] proposed the formula, for a sphere,

$$C_{df}/C_d = BRe^{-m} \quad (14)$$

with $B = 5.48$, $m = 0.50$, and $C_d = C_{df} + C_{dp}$. However, this is only valid for critical Reynolds numbers (see Fig 3), $Re \sim 10^5$, but raindrops have Re values in the range (1500-5000). Beard and Chuang [1] also referred to data from LeClair [8] which provides drag coefficients at low Reynolds numbers. Since there are no experimental values in the desired range of Re, Beard and Chuang did a linear interpolation between Achenbach's and LeClair's data.

Fig 4 shows the points selected from [7], and Fig 5 shows the region of Re between data provided by [7] and [8]. Rather than use the linear interpolation method used in [1], a possibly more accurate 4th-order polynomial fit was used. Only this and the 5th-order fits were suitable for moderate power polynomials, but the 4th order is lower.

Since the graph in Fig 5 is ln-ln, the empirical formula for the pressure drag coefficient is

$$C_{dp} = C_d\left(1 - e^{P(x)}\right) \quad (15)$$

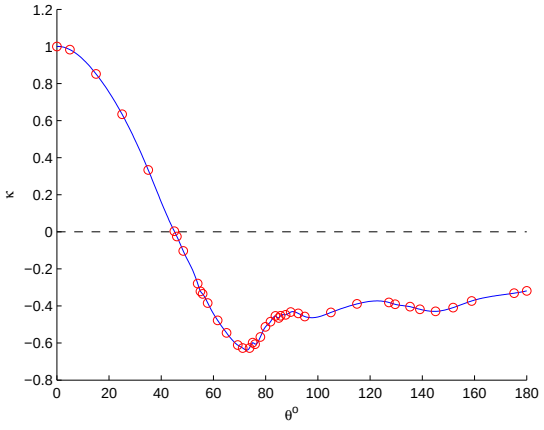

FIG. 2: Experimental data of the dimensionless pressure distribution, around a sphere, for $Re = 157200$, from [5] and its cubic spline interpolation. The Reynolds number is in the critical regime (see Fig 3).

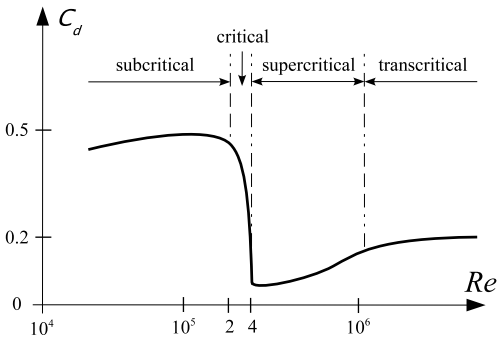

FIG. 3: Drag coefficient of a sphere explaining the four flow regimes. So Fage's results are only for the narrow range.

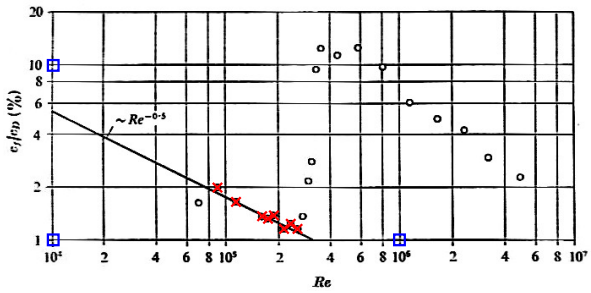

FIG. 4: Since no tabulated data was provided in [7], this graph was scanned and necessary points extracted from the raster image after some callibration.

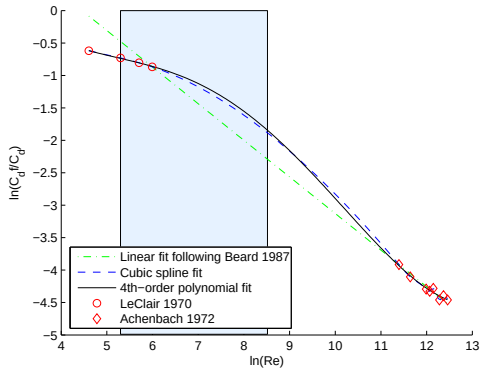

FIG. 5: Frictional drag within the region of interest (shaded in blue).

where

$$P(x) = P_0 + P_1 \ln x + P_2(\ln x)^2 + P_3(\ln x)^3 + P_4(\ln x)^4 \tag{16}$$

and $P_0 = 5.7$, $P_1 = -3.7$, $P_2 = 0.8$, $P_3 = -0.078$, and $P_4 = 0.0025$.

It is appropriate to calculate Re from a sphere of equivalent volume rather than directly from the shape of the raindrop of its oblate spheroid approximation, since the resulting fractional error is only 0.01.

III. CALCULATIONS ADJUSTED FOR SHAPE

1. *Pressure distribution around a spheroid.*

Since the raindrop gets flattened from a sphere, the equations that apply to spheres should be adjusted to an oblate spheroid. The pressure distribution around a spheroid can be first investigated using potential flow to determine the velocity at the surface. Using the techniques of complex potentials as in [9], the potential, in the z-plane, for streaming flow past a sphere can be determined to be

$$\underline{w} = -U_0\left(\underline{z} + \frac{q^2}{\underline{z}}\right) \tag{17}$$

Even though, strictly, the complex potential applies to two-dimensional flow, since this problem is axisymmetric, it is possible to extend this to a sphere [10]. The stream function and velocity potential for a sphere are thus

$$\psi = \frac{1}{2}U_0 r^2 \sin^2\theta\left(1 - \frac{q^3}{r^3}\right) \tag{18a}$$

$$\phi = U_0\left(r\cos\theta + \frac{a^3\cos\theta}{2r^2}\right) \tag{18b}$$

This potential can then be subjected to a conformal transformation to the oblate spheroidal coordinates (see Appendix A 4), giving the surface velocity as

$$U_\eta = U_0 \sin\eta[(\lambda^2+1) - \sin^2\eta]^{-1/2}[(\lambda^2+1)cot^{-1}\lambda - \lambda]^{-1} \tag{19}$$

where λ is the ratio of the axis ratio to the eccentricity $\lambda = \alpha/\epsilon$, $\epsilon = (1-\alpha^2)^{-1/2}$.

Once the velocity at the surface is known, the pressure can be determined by Bernoulli's principal

$$\begin{aligned} B = p_0 + \frac{1}{2}\rho_a U_0^2 &= p(\theta) + \frac{1}{2}\rho_a U(\theta)^2 \\ &= p(\eta) + \frac{1}{2}\rho_a U_\eta^2 \end{aligned} \tag{20a}$$

where the last part of the equation represents pressure and velocity in oblate spheriodal coordinates. The dimensionless pressure is thus

$$\chi_\alpha(\eta) = 1 - \frac{U_\eta^2}{U_0^2} \tag{21}$$

To use this to get a correction for the pressure distribution, we assume that the fractional deviation of the corrected pressure from Fage's measurements for a sphere are the same as the fractional deviation in potential flow around an oblate spheroid from a sphere. Using the stagnation point as reference, this is defined as $[1 - K(\psi)]/[1 - \kappa(\psi)] = [1 - \chi_\alpha(\psi)]/[1 - \chi(\psi)]$, where $K(\psi)$ is the corrected pressure and $\chi(\psi) = 1 - \frac{9}{4}\sin^2\psi$ is the pressure distribution around a sphere. So the corrected pressure is

$$K(\psi) = 1 - \Gamma_\alpha[1 - \kappa(\psi)] \tag{22}$$

where, from potential flow

$$\Gamma_\alpha = [1-\chi_\alpha(\psi)][1-\chi(\psi)]^{-1} = [U_\eta(\psi)/V]^2 \left[\frac{9}{4}\sin^2\psi\right]^{-1} \tag{23}$$

Starting with $\tan\eta = \alpha^{-1}\tan\psi$, and using $tan\eta = y_\eta/x_\eta$ such that $\sin\eta = y/(x_\eta^2+y_\eta^2)^{-1/2}$, we have

$$\begin{aligned}
\sin^2\eta &= \frac{y_\eta^2}{x_\eta^2+y_\eta^2} && \text{(24a)}\\
&= \frac{1}{cot^2\eta+1} && \text{(24b)}\\
&= \frac{1}{(\alpha\cot\psi)^2+1} && \text{(24c)}\\
&= \frac{\sin^2\psi}{\alpha^2\cos\psi+\sin^2\psi} && \text{(24d)}
\end{aligned}$$

which can be substituted into Eq (23) to give the adjustment factor of

$$\Gamma_\alpha = \frac{4}{9}\lambda^{-2}[(\lambda^2+1)\cot^{-1}\lambda-\lambda]^{-2} \tag{25}$$

since $\lambda = \alpha[1-\alpha^2]^{-1/2}$.

It is important to note that separation of flow occurs around a raindrop after a certain angle, just like it does for a sphere. So the potential flow solution is valid only for the unseparated flow region, which is from 0^o to 72^o. In the wake region, 88^o to 180^o, the adjustment is taken to be a constant $\Gamma = \Gamma_d$, which is determined by balancing the drag in Eq (12a) with the drag from the empirical relation, Eq (15). The transition region in between is just assumed to be a linear transition from Γ_α to Γ_d.

To summarize, the value of Γ depends on the angles as

- 0 to 72^o: unseparated flow, Γ_α given by (25)
- 72^o to 88^o: simple linear transition
- 88^o to 180^o: wake, constant adjustment $\Gamma = \Gamma_d$

2. *Raindrop shape using an intermediate force method*

Finally, it remains for the weight of raindrop to equal the drag force. This is accomplished by using the intermediate forcing method introduced in [1], composed of both the increased drag and "reduced-weight" methods. This involves changing b from Eq (8) to

$$b = [c'\Delta\rho g/\sigma]^{1/2} \tag{26}$$

where $c' = 0.5(1+C_{dp}/C_d)$, and multiplying the corrected pressure distribution with an amplitude factor to become $\Lambda K(\psi)$, to satisfy the lower boundary condition.

IV. PROCEDURE

A. Initialization

To test the implementation of the model, certain parameters should be initialized. There were two ways that were employed

- From tables in Beard and Chuang's paper [1]
- From a photo of a raindrop from Magono's paper [2]

From the tables, diameters, d, can be chosen, and fall velocities, U_0 can be determined to provide the appropriate Re values. The axis ratio, α, pressure amplitude, Λ, and wake adjustment, Γ_d can be initialized using values the same row as d. From the photo, the boundary of the raindrop is determined via edge-detection techniques and a curve plot determined. From this vector plot, the width, w, and axis ratio of the drop can be measured. Also, the diameter of the equivalent volume sphere can be calculated from the relation $V = \pi/6d^3 = \alpha\pi/6w^3$ to give

$$d = \alpha^{1/3}w \tag{27}$$

The remaining parameters, Λ, and Γ_d can be estimated from the appropriate rows in tables of [1].

B. Requirements

The solution of the shape of the raindrop by integrating Eq (10) involves quite a number of iterations and repetitions before a final steady solution is reached. Basically, this has been broken down into three actions:

- Balance volume,
- Balance drag, and
- Balance weight

Balancing the volume requires the raindrop, corresponding to a sphere of diameter d, has the same volume as the latter. This is accomplished by iterating values of R_t under a bracketing root finding scheme. Balancing the drag force requires that C_d is adjusted in Eq (12a) until the drag coefficient is equal to that in the empirical formula Eq (15). Balancing the weight requires that the amplitude factor Λ for the pressure distribution $\kappa(\psi)$ is moderated until the drag force (Eq (13) is equal to the weight, $W = V\rho g$ of the raindrop. All methods have to utilize bracketing root finding schemes, since the derivatives of their functions are unknown.

Idealy, repeated application of these steps should allow the shape to converge to a steady state with closure at the bottom pole. However, this was not found to be for the program implemented. Therefore, an alternative to the balancing of the weigh has been introduced. As it is more important for the shape to be closed, a fourth action performs the following

- Close shape

This is done by increasing Λ from a small value until just before the shape is open at the bottom pole.

C. Executable stages

With the preceding requirements, the program has been broken down into 6 executable stages. Having performed the initializations, these are the steps to obtain the shape of a raindrop

1. Run to iterate R_t, to balance volume
   - produces values for R_t, cross-sectional area, A, and α
   - which should be set to prepare for Stage 2
2. Run to iterate Γ_d, to balance drag
   - produces value for Γ_d
   - which should be set to prepare for Stage 4
3. *Run to iterate* Λ*, to balance weight* **(NOT USED)**
4. Run to increment Λ, to close shape
   - produces value for Λ
   - which should be set to prepare for Stage 5
5. Run to print summary result
6. Run to print coordinate points to be used for plotting

Note that, unfortunately, the drag force would not equal the weight.

D. Issues

Due to anomalies in the program, one major issue was the inability to have convergent drag forces and weights. Even though this currently provides strictly non-physical answers, this problem can be resolved given time such that the requirements as in [1] can be satisfied.

Another issue was the error margins used in the program. Due to the lack of time and computing resources, larger error margins were used in calculations than in [1]. An artifact of this leniency is the jaggedness in the change in shape with respect to the parameters when observed at high resolutions. This leads to root finders occasionally complaining that the functions are discontinuous. The error bounds used are as follows

TABLE I: Error constraints set in the C program

Name	Value
RES_DEG	1
BRACKET_ERR	1.0e-6
NEWTON_ERR	1.0e-5
INTEGRATION_ERR	1.0e-5
ERR_PHI	1.0e-4
ERR_PHI_FACTOR	10

Also, the stages were run only once per result, so the results would contain some significant error. If there was more time, a scheme for running the stages multiple times could be developed to allow for more stable solutions.

E. Physical constants

The following are the physical constants used in the program, from [11].

TABLE II: Error constraints set in the C program

Physical constant	Value
Water-air surface tension, σ	72.75 dynes/cm
Water density (at 20^{o}C), ρ_w	0.99821 gm/cm^3
Air density (at 300K, 1 bar), ρ_a	1.161 kg/m^3
Air viscosity (at 300K, 1 bar), μ_a	18.6 μPa-s
Standard gravity, g	9.80665 m/s^2

V. RESULTS

A. *d* = 1, 2, 3, 4, 5, and 6 mm

After calculating a few million points and selecting only those at integer degree tangent angle increments, the raindrop shapes are plotted and shown in Fig 6. Notice that larger raindrops have smaller axis ratios and all shapes have the points of largest curvature below the center horizontal line.

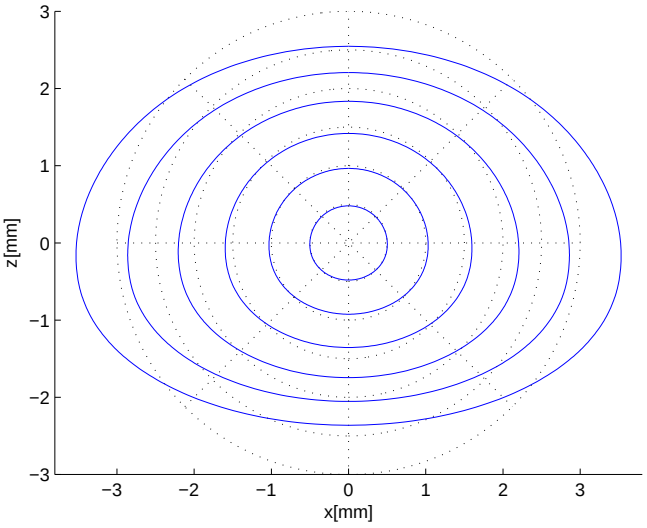

FIG. 6: Drop shape for d = 1, 2, 3, 4, 5, and 6 mm with origin at center of volume. Shown for comparison are dashed circles of diameter d.

TABLE III: Raindrop size parameters (Re), model axis ratios α, volume V and cross-sectional area A, with the pressure distribution adjusted for drag and distortion (Γ_d, Λ), and drag force and weight (D, W).

d (mm)	Re	α	V(mm^3)	A (mm^2)	R_t (m)	Γ_d	Λ	D (N)	W (N)
1.0	263	0.958	0.510	0.791	0.507	0.731	3.102	0.0021	0.0050
2.0	863	0.916	4.238	3.339	1.067	0.869	0.992	0.0283	0.0414
3.0	1593	0.868	14.956	8.022	1.721	1.044	0.591	0.1136	0.1462
4.0	2267	0.811	36.822	15.295	2.518	1.233	0.455	0.2777	0.3600
5.0	3012	0.744	73.805	25.716	3.534	1.381	0.418	0.5157	0.7217
6.0	3625	0.695	129.603	39.165	4.793	1.615	0.374	0.8103	1.2672
7.0	4230	0.636	204.228	56.116	6.425	1.708	0.372	1.1840	1.9969
8.0	4834	0.572	315.783	80.270	8.924	1.928	0.343	1.7210	3.0877

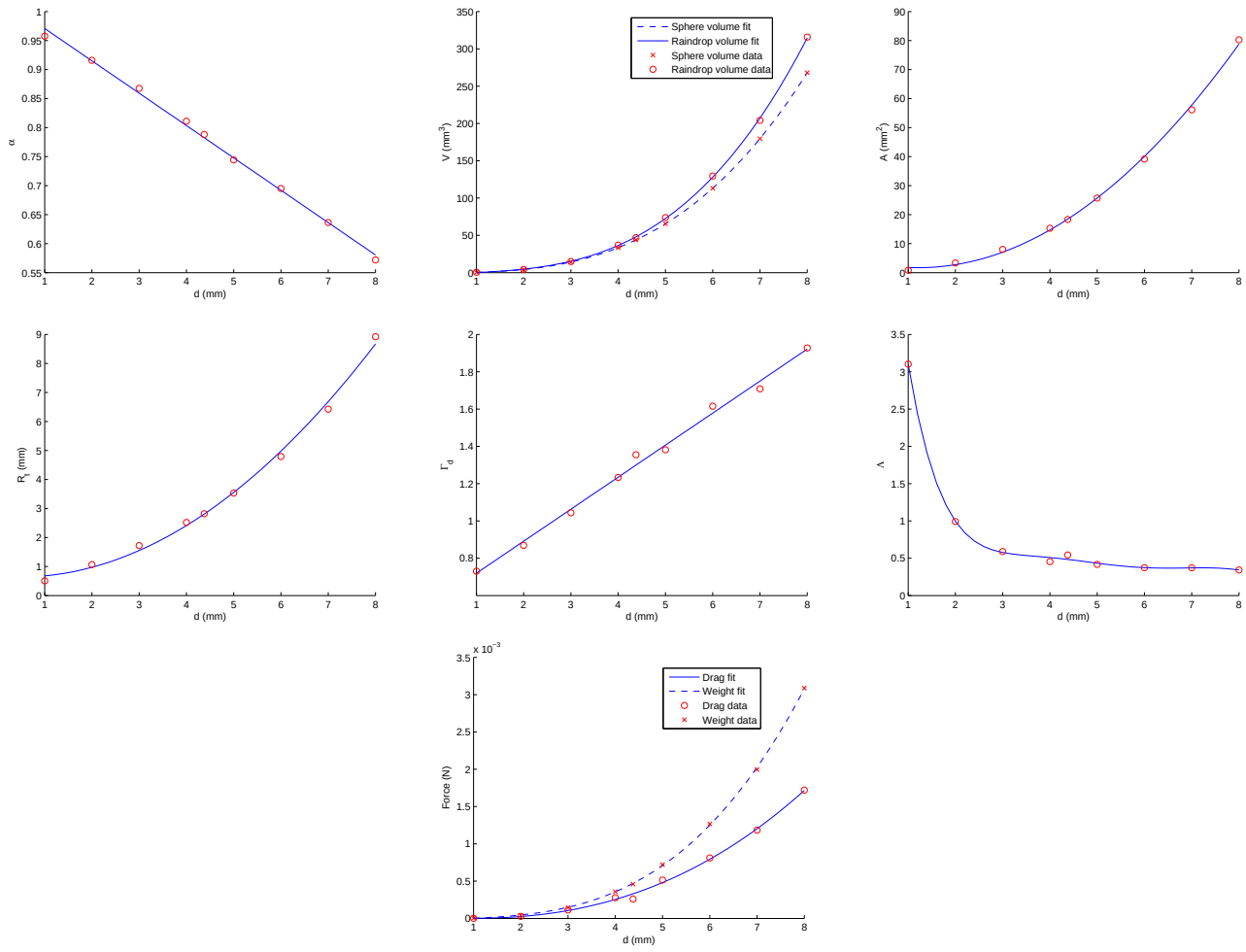

FIG. 7: Graphs illustrating the relationships of the axis ratio, program parameters, and physical properties with respect to sphere diameter. The nth-order polynomial (P_n) fits are: $\alpha \sim P_1(d)$, $V_s \sim P_3(d)$, $V \sim P_3(d)$, $A \sim P_2(d)$, $R_t \sim P_2(d)$, $\Gamma_d \sim P_1(d)$, $\Lambda \sim P_6(d)$, $D \sim P_3(d)$, $W \sim P_3(d)$.

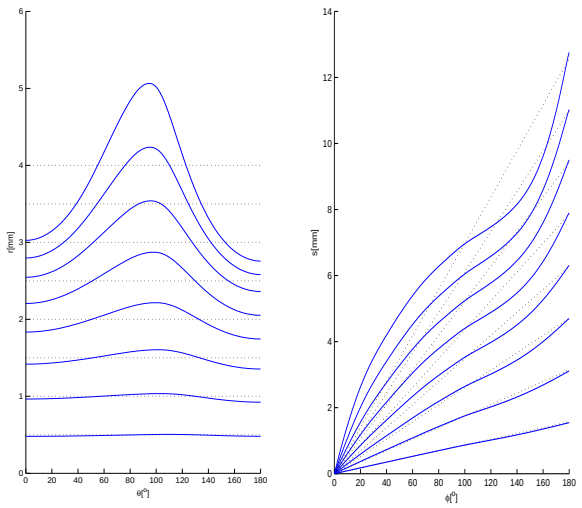

FIG. 8: Deviations from circle lines in polar r-θ (left) tangential s-ϕ (right) and coordinates mapped in the cartesian plane, for d = 1, 2, 3, 4, 5, 6, 7, and 8 mm.

Input parametric values and results for integer mm values of the equivalent-volume sphere diameter d and are shown in Table III, and represented in Fig 7. As can be seen from the graphs, the axis ratio, α, decreases linearly with increasing d, and the radius of curvature at the top. In accordance with dimensionality, the raindrop volume, V, increases as a cubic function in d, and the cross-sectional area, A, increases as a quadratic function in d. One can see that because of the non-conservation of weight in the failure of Stage 3 of the program procedure, the calculated raindrop shape grows faster than the volume of the sphere. This can also be observed for the divergence between the weight of the raindrop, W, and the drag force on it, D. It is interesting to note that the configuration parameters, R_t, and Γ_d, are quadratic, and linear functions of d, respectively. However, Λ requires a 6th-order polynomial fit for its values, given the excessively high value for $d = 1.0$mm.

Fig 8 shows the polar and tangential coordinates for raindrops of varying sizes and their equivalent-volume spheres in the cartesian representation. Deviations from the lines for spheres increase for larger raindrops.

B. Raindrop of width 4.8mm

The case for a raindrop of width, w, 4.8mm and speed, U, 8.3m/s is more thoroughly discussed in this section and compared against photographic evidence provided in [2]. The scanned photograph of the raindrop is analyzed and the contour of the raindrop edge-detected to produced a vectorized curve (see Fig 9). From the curve, and knowing that the width of the raindrop is specified to be 4.8mm, the diameter of the equivalent-volume sphere, d, is determined to be 4.36mm. The model is then calculated for these d and U values.

The raindrop contour from the photograph has been sized to the same scale as that of the model, by a w/x_{span} factor, where, where x_{span} is the width of the contour curve in pixels. The estimated center of volume of the raindrop contour has also been shifted to the origin (though possibly slightly too high) to compare appropriately with the model. Fig 10 shows that the top portion of the model fits quite well with the photo, while the bottom portion is too low. This lack of flatness at the bottom was verified with the lower drag values to the weights as shown in the last graph of Fig 7. Had the drag been raised to balance the weight, the bottom portion should be flatter. Thus the axis ratio the model predicts is a little too large.

A 3D model of the raindrop is shown in Fig 11 to provide a better perspective of what the raindrop would look like physically, according to the model.

VI. COMPARISON AGAINST ORIGINAL PAPER, BEARD AND CHUANG 1987

A. *d* = 5.0mm

Choosing $d = 5.0$mm, we can compare a particular result of this implementation of the model with the original [1] (see Table IV). As can be seen, the axis ratio for the current model is a little too large, the Γ_d constant also too big, and the Λ amplitude too low, therefore giving higher weight than drag. Fig

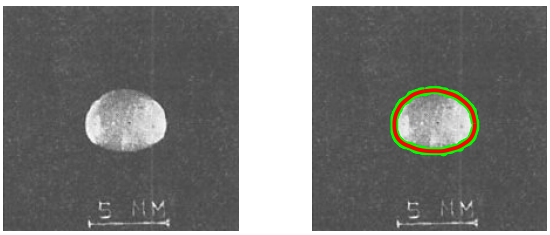

FIG. 9: Photos from [2], with the left showing the original and the right showing the edge-detected boundary of the raindrop used for comparison with model.

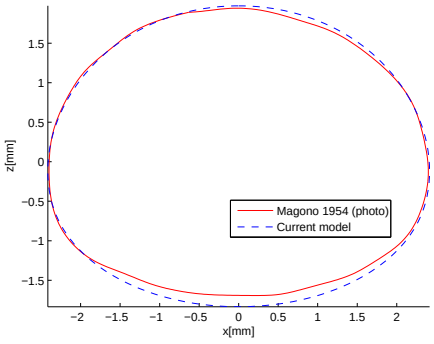

FIG. 10: Comparison of model with photograph of a raindrop of width 4.8mm, $U = 8.3$m/s, from [2].

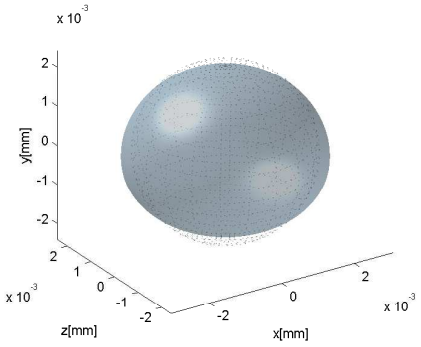

FIG. 11: 3D rendering of a raindrop of $d = 4.3755$mm, $U = 8.3$m/s, $Re = 2267$, corresponding to the photograph in Fig 9. A wireframe of a sphere of diameter d is also overlayed.

12 and Fig 13 show graphically that the implemented model is flatter than the original, but its width is just only slightly larger.

TABLE IV: Comparison of models in this project with the original [1] for $d = 5.0$mm, $Re = 3021$.

Source	α	Γ_d	Λ
Lim	0.744	1.381	0.418
Beard and Chuang	0.694	1.050	0.778

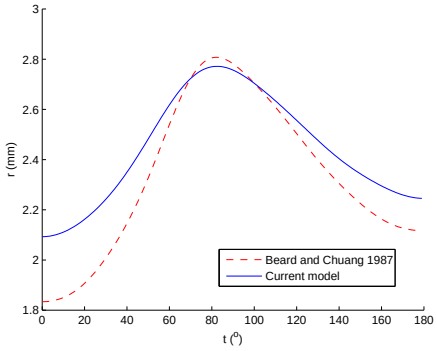

FIG. 12: Comparison of polar coordinates between implemented and original models.

B. Shape coefficients, c_n

A more rigorous method to compare the models would be to Fourier analyze of each shape. The drop surface can be represented by a cosine series distortion on a sphere

$$r = q\left(1 + \sum_{n=0}^{10} c_n \cos n\theta\right) \tag{28}$$

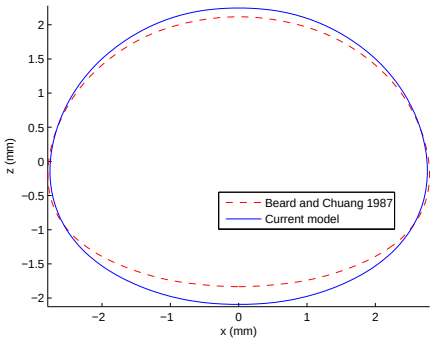

FIG. 13: Comparison of shape between implemented and original models.

where $q = a_0/2$, is the sphere radius, and $c_n = a_n/q$, with a_n the Fourier cosine coefficients as in Appendix C 6, and c_n are the deformation or shape coefficients. Table VI lists the coefficients for d =1, 2, 3, 4, 5, 6, 7, and 8mm. Diameters d =1, 2, 3, 4, 5, and 6mm were compared against those of [1], and the differences compiled in Table V. Fig 14 shows a bar chart for $d = 5.0$mm. The discrepancy between the models are not too big, and the differences converge for small raindrops, as expected, since small raindrops approximate to spheres.

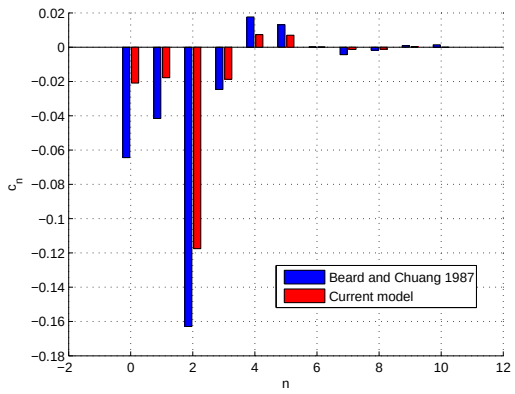

FIG. 14: Comparison of shape coefficients between implemented and original models.

TABLE V: Comparison of shape coefficients from the implemented model (c_n') with Beard and Chuang (c_n). Deviations in percentage are computed from $\Delta c_n = c_n - c_n'$.

d (mm)	$\sum \lvert\Delta c_n\rvert$	$\sum \lvert c_n\rvert$	$\sum \lvert\Delta c_n\rvert \,/\, \sum \lvert c_n\rvert \times 100\%$
2.0	0.017	0.075	22.3
3.0	0.047	0.151	31.2
4.0	0.094	0.246	38.1
5.0	0.141	0.333	42.3
6.0	0.197	0.421	46.7

TABLE VI: Coefficients from the cosine series fit to the computed shapes.

	Shape coefficients [$c_n \times 10^4$]										
d (mm)	$n=0$	1	2	3	4	5	6	7	8	9	10
1.0	-164	83	-216	-80	-13	10	6	0	-2	-1	1
2.0	-119	-103	-446	-128	-12	19	2	-4	-10	-4	-4
3.0	-66	-81	-712	-157	12	39	8	-2	-6	1	1
4.0	-69	-88	-1049	-186	49	57	3	-11	-12	-1	-2
5.0	-209	-178	-1175	-187	73	70	1	-13	-12	3	-1
6.0	-153	-168	-1462	-202	124	90	-4	-22	-14	6	0
7.0	-242	-206	-1783	-172	199	95	-24	-34	1	8	-4
8.0	-451	-223	-2157	-151	315	117	-45	-47	-10	22	0

VII. NOMENCLATURE

A	cross-sectional area of raindrop
b	inverse length intrinsic to Laplace's equation [=$\sqrt{\Delta\rho g/\sigma}$]
B	Bernoulli constant along a streamline
C	dimensionless radius of curvature at the top pole [=bR_t]
c'	adjustment constant on b for mean forcing method
C_d	total drag coefficient
C_{df}	friction drag coefficient
C_{dp}	pressure drag coefficient
d	diameter of equivalent volume sphere
D	drag force on raindrop
g	acceleration due to gravity (standard gravity)
p_e	external pressure
p_i	internal pressure
q	radius of equivalent volume sphere [=$d/2$]
Q	dimensionless radius of equivalent volume sphere [=bq]
Re	Reynolds number
R_1, R_2	orthogonal radii of curvature
R_t	radius of curvature at the top pole
s	arc length measured from the top pole
S	dimensionless arc length measured from top pole [=bs]
SA	surface area of raindrop
U_0	raindrop fall velocity
V	volume of raindrop
w	width of raindrop
W	weight of raindrop
We	Weber number
X	dimensionless x-coordinate [=bx]
Z	dimensionless z-coordinate [=bz]
α	axis ratio of raindrop
Γ	flow adjustment for distortion around oblate spheroid
Γ_α	potential flow adjustment around oblate spheroid
Γ_d	pressure drag adjustment around oblate spheroid
η	elliptic hyperbola coordinate
ϕ	tangent angle measured from the horizontal at the top pole
$\kappa(\psi)$	dimensionless pressure distribution around a sphere
$K(\psi)$	dimensionless corrected pressure distribution adjusted for distortion around oblate spheroid
μ_a	dynamic viscosity of air
Δp	pressure difference across drop surface [=$_i - p_e$]
$\Delta\rho$	density difference between water and air [=$\rho_w - \rho_a$]
θ	polar angle measured from bottom pole
σ	water-air surface tension
ξ	elliptic ellipse coordinate
ψ	tangent angle measured from the horizontal from the bottom pole

APPENDIX A: COORDINATE GEOMETRY

1. Curvature

Of interest in this paper is the basic extrinsic curvature, with particular attention to the radius of curvature. The radius of curvature, analogous to the radius of a circle, is defined by the differential relation $ds = rd\theta$ where s is the arc length and θ the angle between two subtended radii to the arc, as shown in Fig 15. The curvature is simply defined as $\rho = 1/r$, so

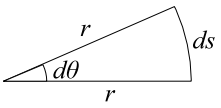

FIG. 15: A curvilinear rectangular element of a surface separating two fluids (adapted from [12]

$$\rho = 1/r = \frac{d\theta}{ds} \tag{A1}$$

In 3D, there would be two radii of curvature defined by any two orthogonal arcs at each point on the surface. See Fig 22.

2. Tangential Coordinate System

Following the explanations in [13], this section describes the tangential coordinate system used to calculate the shape of a raindrop.

For an arbitrarily curved surface, there would be two principal curvatures at every point due to arcs on the surface orthogonal to each other. Considering only axisymmetric surfaces, it is convenient to take one curvature in the meridional cross section, so that $ds = r_1 d\phi$, where s is the arc length from the origin, defined as the 'top' pole, and θ the angle between the tangent at the surface to the horizontal. See Fig 16. The curvature is then

$$\frac{1}{r_1} = \frac{d\phi}{ds} \tag{A2}$$

Fig 17 demonstrates the tangential coordinate system with a circle in cartesian coordinates, with tangential parameters, and maps them to a cartesian representation. Notice that the $\phi(s)$ function is always monotonic since both ϕ and s can only increase.

The other principal curvature is determined from the zonal cross section, noting from Fig 17 that $x = r_2 \sin\phi$, such that the curvature is

$$\frac{1}{r_2} = \frac{sin\theta}{x} \tag{A3}$$

Referring to the differential relation illustrated in the insert

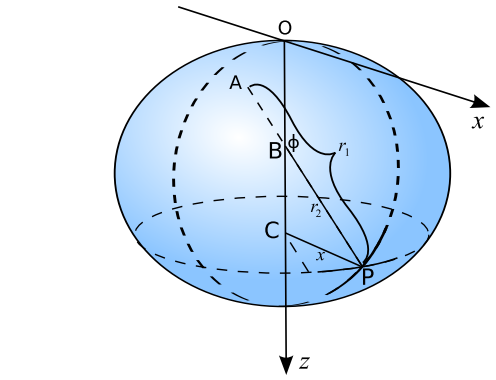

FIG. 16: 3D diagram showing curvatures

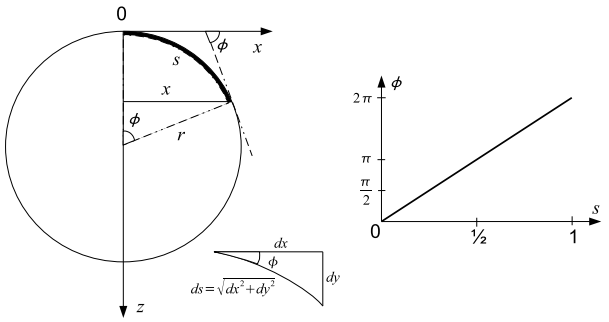

FIG. 17: Diagram showing a circle in cartesian coordinates with tangential parameters and in tangential coordinates. Note that $\phi(S)$ is monotonic.

of Fig 17, it follows that

$$\frac{dx}{ds} = \cos\theta \tag{A4a}$$

$$\frac{dy}{ds} = \sin\theta \tag{A4b}$$

$$\frac{dy}{dx} = \tan\theta \tag{A4c}$$

3. Elliptic Coordinate System

Starting with elliptical coordinates[14], the oblate spheroidal coodinates can be derived. This system defines coordinates in terms of confocal ellipses and hyperbolas. The ellipse coordinate, ξ, is defined with the semi-major axis of the ellipse, $a_e = (d_1 + d_2)/2$, while the hyperbola coordinate system is defined with distance between x-intercepts of the hyperbola, $a_h = (d_1 - d_2)/2$. Thus the coordinates are

$$\xi = \frac{a_e}{f} = \frac{d_1 + d_2}{2f} \tag{A5a}$$

$$\eta = \frac{a_h}{f} = \frac{d_1 - d_2}{2f} \tag{A5b}$$

where d_1 and d_2 are the distances from the foci to the point of interest, and f is the distance from the center to each focus.

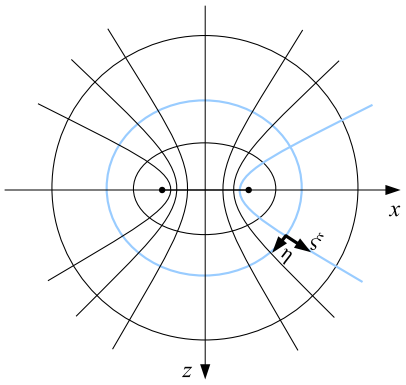

FIG. 18: Elliptic coordinate system with coordinates ξ and η representing ellipses and hyperbolas.

We thus have, for the ellipse

$$a_e = f\xi \tag{A6a}$$
$$b_e = a_e^2 - f^2 = f\sqrt{\xi^2 - 1} \tag{A6b}$$

and for the hyperbola

$$a_h = f\eta \tag{A7a}$$
$$b_h = f^2 - a_h^2 = f\sqrt{1 - \xi^2} \tag{A7b}$$

a. *Elliptic to Cartesian Coordinates*

Substituting ξ and η into the cartesian equations for ellipse, and hyperbola

$$(x/a_e)^2 + (z/b_e)^2 = 1 \tag{A8a}$$
$$(x/a_h)^2 - (z/b_h)^2 = 1 \tag{A8b}$$

we get

$$\frac{x^2}{\xi^2} + \frac{z^2}{\xi^2 - 1} = f^2 \qquad (1 < \xi < \infty) \tag{A9a}$$
$$\frac{x^2}{\eta^2} + \frac{z^2}{1 - \eta^2} = f^2 \qquad (-1 < \eta < 1) \tag{A9b}$$

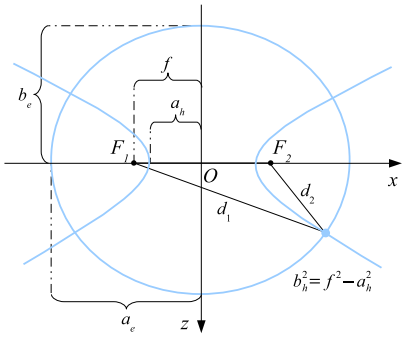

FIG. 19: Parameters associated with ellipses and hyperbolas.

Solving Eqs A9a and A9b for x and z produce the Cartesian-Elliptical coordinates relations

$$x = f\xi\eta \tag{A10a}$$
$$z = f\sqrt{(\xi^2 - 1)(1 - \eta^2)} \tag{A10b}$$

b. *Elliptic to Polar Coordinates*

To map the elliptic coordinates to polar coordinates, consider the asymptotes of the hyperbolas. The angle the asymptote in the first quadrant makes with the x-axis for the hyperbola, $(x/a_h)^2 - (z/b_h)^2 = 1$ is defined as $\tan\varphi = b_h/a_h$. From Eq A9b, this means

$$\tan\varphi = \frac{\eta}{\sqrt{1 - \eta^2}} \tag{A11a}$$
$$\cos\varphi = \eta \tag{A11b}$$

From Fig 20, the polar angle to the point of interest is defined as $\tan\theta = x_e/z_e$, while the angle for the asmyptote is $\tan\varphi = x_e/z_c$. Dividing the two tangents, we get

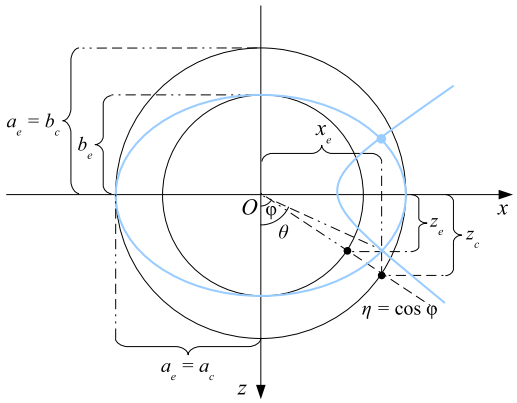

FIG. 20: Relating elliptic coordinates to polar coordinates.

$$\frac{\tan\varphi}{\tan\theta} = \frac{z_e}{z_c} = \frac{b_e}{b_c} = \frac{a_e}{b_e} = \alpha \tag{A12}$$

So we have the relation to be used, $\tan\varphi = \alpha\tan\theta$.

c. *Elliptic to Tangential Coordinates*

To relate the elliptic coordinates to tangential coordinates referenced to the lower pole, consider the cartesian equation of the ellipse, $(x/a_e)^2 + (z/b_e)^2 = 1$, and taking a derivative with respect to z

$$\frac{2x}{a_e^2} + \frac{2z}{b_e^2}z' = 0 \tag{A13}$$

Where $z' = dz/dx$. Rearranging and substituting for the point of interest, as shown in Fig 21

$$z' = -\frac{b_e^2}{a_e^2}\frac{x_e}{z_e} = -\alpha^2\tan\theta \tag{A14}$$

Since, z' is the gradient of the tangent line, making an angle psi' with the x-axis, we have $z' = -\tan\psi$, which gives

$$\tan\psi = \alpha^2 \tan\theta \tag{A15}$$

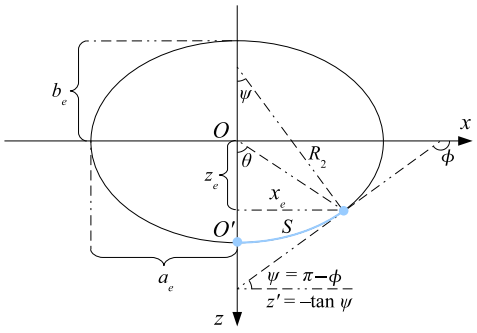

FIG. 21: Relating elliptic coordinates to tangential coordinates referenced to the lower pole.

4. Oblate Spheroidal Coordinate System

This is just the revolving of the elliptic coordinate system about the z-axis and leads to the following expressions

$$x = f\xi\eta\sin\theta \tag{A16a}$$
$$y = f\xi\eta\cos\theta \tag{A16b}$$
$$z = f\sqrt{(\xi^2-1)(1-\eta^2)} \tag{A16c}$$

where θ is the polar angle.

APPENDIX B: EXTENDED DERIVATIONS

1. The Laplace-Young equation

The following is an adaptation from the derivation given in [12].

Work done by excess pressure

$$\delta W = \Delta p S \delta r \tag{B1}$$

Increase in surface energy

$$\delta U = \sigma \delta S \tag{B2}$$

Subst. x and y

$$\delta U = \sigma[(x+\delta x)(y+\delta y) - xy] \tag{B3}$$

Using similarity of triangles $O_1A'B'$ and O_1AB

$$\frac{x+\delta x}{r_1+\delta r} = \frac{x}{r_1} \tag{B4}$$

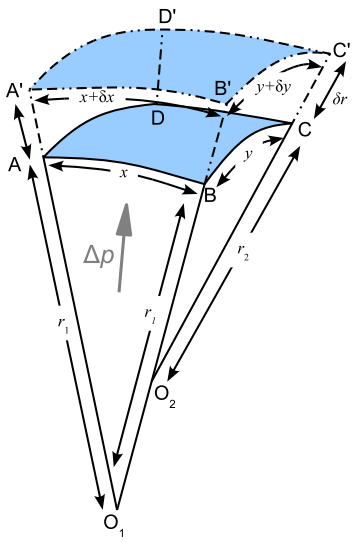

FIG. 22: A curvilinear rectangular element of a surface separating two fluids (adapted from [12]

Thus

$$x + \delta x = x\left(1 + \frac{\delta r}{r_1}\right) \tag{B5}$$

Similarly for $O_2B'C'$ and O_2BC

$$y + \delta y = y\left(1 + \frac{\delta r}{r_2}\right) \tag{B6}$$

Subst. into Eq (B3)

$$\begin{aligned}\delta U &= \sigma\left[xy\left(1+\frac{\delta r}{r_1}\right)\left(1+\frac{\delta r}{r_2}\right) - xy\right] \\ &= \sigma xy\delta r\left(\frac{1}{r_1}+\frac{1}{r_2}\right) + O(\delta r^2) \\ &= \sigma S\delta r\left(\frac{1}{r_1}+\frac{1}{r_2}\right) + O(\delta r^2)\end{aligned} \tag{B7a}$$

where $S = xy$.

Equating (B1) to (B7a), neglecting quadratic terms in change

$$\Delta p S\delta r = \sigma S\delta r\left(\frac{1}{r_1}+\frac{1}{r_2}\right) \tag{B8}$$

$$\Delta p = \sigma\left(\frac{1}{r_1}+\frac{1}{r_2}\right) \tag{B9}$$

APPENDIX C: NUMERICAL METHODS

1. 4th-Order Runge-Kutta Method

The differential equations governing the drop shape are integrated using a 4th-order Runge-Kutta scheme.

a. Classical Runge-Kutta Method

The classical method [18] is summarized as

$$k_1 = hf(x_n, y_n), \quad \text{(C1a)}$$
$$k_2 = hf(x_n + \frac{h}{2}, y_n + \frac{h}{2}k_1), \quad \text{(C1b)}$$
$$k_3 = hf(x_n + \frac{h}{2}, y_n + \frac{h}{2}k_2), \quad \text{(C1c)}$$
$$k_4 = hf(x_n + \frac{h}{2}, y_n + k_3), \quad \text{(C1d)}$$

$$\Delta y_n = \frac{1}{6}\left(k_1 + 2k_2 + 2k_3 + k_4\right) \quad \text{(C2)}$$

$$y_{n+1} = y_n + \Delta y_n \quad \text{(C3)}$$

where $y' = f(x, y)$ is the function derivative of y, h, is the step size, which should be small, and$y(x_0) = y_0$ is the initial condition.

b. Modified Runge-Kutta Scheme

However, due to the combination of variables from cartesian and tangential coordinate systems in Eq (10), the Runge-Kutta method has to be modified, as done by Hartland and Hartley (1976).

The system of differential equations are repeated here

$$\frac{d\phi}{dS} = \frac{2}{C} + Z - \frac{\sin\phi}{X} - \frac{We}{Q}[\kappa(\pi - \phi) - \kappa(\pi)] \quad \text{(C4)}$$

$$\frac{dX}{dS} = \cos\phi \quad \text{(C5)}$$

$$\frac{dZ}{dS} = \sin\phi \quad \text{(C6)}$$

with boundary conditions

$$\frac{d\phi}{dS} = \frac{\sin\phi}{X} = \frac{1}{C} \quad \text{(C7)}$$

where $X = Z = \phi = 0$.

$$\frac{dV}{dS} = \pi X^2 \sin\phi \quad \text{(C8)}$$

$$\frac{dA}{dS} = 2\pi X \quad \text{(C9)}$$

For a step length $h = \Delta S$, increments in ϕ, x, z, V, and A are given by

$$\Delta\phi = \frac{1}{6}(\Delta\phi_1 + 2\Delta\phi_2 + 2\Delta\phi_3 + \Delta\phi_4) \quad \text{(C10a)}$$
$$\Delta X = \frac{1}{6}(\Delta X_1 + 2\Delta X_2 + 2\Delta X_3 + \Delta X_4) \quad \text{(C10b)}$$
$$\Delta Z = \frac{1}{6}(\Delta Z_1 + 2\Delta Z_2 + 2\Delta Z_3 + \Delta Z_4) \quad \text{(C10c)}$$
$$\Delta V = \frac{1}{6}(\Delta V_1 + 2\Delta V_2 + 2\Delta V_3 + \Delta V_4) \quad \text{(C10d)}$$
$$\Delta A = \frac{1}{6}(\Delta A_1 + 2\Delta A_2 + 2\Delta A_3 + \Delta A_4) \quad \text{(C10e)}$$

where

$$\begin{aligned}
\Delta\phi_1 &= \{2/C + Z - \sin\phi/X \\
&\quad -We[\kappa(\pi - \phi) - \kappa(\pi)]/Q\}\Delta S \\
\Delta X_1 &= \cos\phi\Delta S \\
\Delta Z_1 &= \sin\phi\Delta S \\
\Delta V_1 &= \pi X^2 \sin\phi\Delta S \\
\Delta A_1 &= 2\pi X\Delta S
\end{aligned}$$

$$\begin{aligned}
\Delta\phi_2 &= \{2/C + (Z + \Delta Z_1/2) \\
&\quad -\sin(\phi + \Delta\phi_1/2)/X\}\Delta S \\
&\quad -We[\kappa(\pi - \phi - \Delta\phi_1/2) - \kappa(\pi)]/Q\}\Delta S \\
\Delta X_2 &= \cos(\phi + \Delta\phi_1/2)\Delta S \\
\Delta Z_2 &= \sin(\phi + \Delta\phi_1/2)\Delta S \\
\Delta V_2 &= \pi(X + \Delta X_1/2)^2 \sin(\phi + \Delta\phi_1/2)\Delta S \\
\Delta A_2 &= 2\pi(X + \Delta X_1/2)\Delta S
\end{aligned}$$

$$\begin{aligned}
\Delta\phi_3 &= \{2/C + (Z + \Delta Z_2/2) \\
&\quad -\sin(\phi + \Delta\phi_2/2)/X]\Delta S \\
&\quad -We[\kappa(\pi - \phi - \Delta\phi_2/2) - \kappa(\pi)]/Q\}\Delta S \\
\Delta X_3 &= \cos(\phi + \Delta\phi_2/2)\Delta S \\
\Delta Z_3 &= \sin(\phi + \Delta\phi_2/2)\Delta S \\
\Delta V_3 &= \pi(X + \Delta X_2/2)^2 \sin(\phi + \Delta\phi_2/2)\Delta S \\
\Delta A_3 &= 2\pi(X + \Delta X_2/2)\Delta S
\end{aligned}$$

$$\begin{aligned}
\Delta\phi_4 &= \{2/C + (Z + \Delta Z_3) \\
&\quad -\sin(\phi + \Delta\phi_3)/X]\Delta S \\
&\quad -We[\kappa(\pi - \phi - \Delta\phi_3) - \kappa(\pi)]/Q\}\Delta S \\
\Delta X_4 &= \cos(\phi + \Delta\phi_3)\Delta S \\
\Delta Z_4 &= \sin(\phi + \Delta\phi_3)\Delta S \\
\Delta V_4 &= \pi(X + \Delta X_3)^2 \sin(\phi + \Delta\phi_3)\Delta S \\
\Delta A_4 &= 2\pi(X + \Delta X_3)\Delta S
\end{aligned}$$

The algoritm was implemented in Matlab, where Δ is denoted by D, and ϕ by phi.

2. Search Methods for Solutions at Points of Interest

a. *Solution at Given Angle*

Using the definition of differentiation from first principles

$$\frac{d\phi}{dS} = \lim_{\Delta S \to 0} \frac{(\phi)_{S+\Delta S} - (\phi)_S}{\Delta S} \approx \frac{\Delta\phi}{\Delta S}, \tag{C15}$$

we can find the next step size as

$$\Delta S^* \approx \frac{\phi^* - \phi_n}{(d\phi/dS)_n} \tag{C16}$$

b. *Point of Inflection*

Other points of interest are points of inflection where $d\phi/dS = 0$, shown as stationary points on the ϕ-S graph, like in Fig 17. Here, we also use derive from first principle, for second order differentiation

$$\frac{d^2\phi}{dS^2} = \lim_{\Delta S \to 0} \frac{(d\phi/dS)_{S+\Delta S} - (d\phi/dS)_S}{\Delta S} \approx \frac{\Delta(d\phi/dS)}{\Delta S}, \tag{C17}$$

and since $d\phi/dS$ is zero here,

$$\Delta S^* \approx -\frac{(d\phi/dS)_n}{(d^2\phi/dS^2)_n} \tag{C18}$$

3. Newton-Raphson Method to estimate ΔS at exact ϕ^*, near determined ϕ

The Newton-Raphson method is used to determine ΔS at desired $\Delta\phi$ values. This is required since it is a backward process given that ΔS is actually the parameter in equation C10a.

a. *General Derivation of Newton-Raphson Method*

Consider the Taylor expansion of a function $y = f(x)$

$$y = f(x_\alpha) + f'(x_\alpha)(x - x_\alpha) + f''(x_\alpha)(x - x_\alpha)^2 + \cdots \tag{C19}$$

where f' is the first derivative of f, f'' the second, and so on. Neglecting the nonlinear terms, for small $(x - x_\alpha)$, and rearranging to find the x-intercept when $y = 0$, we get

$$x = x_\alpha - \frac{f(x_\alpha)}{f'(x_\alpha)} \tag{C20}$$

Setting $x_\alpha = x_n$ to be the current iteration for the x-intercept and $x = x_{n+1}$ for the next iteration, we arrive at the recursive relation

$$x_{n+1} = x_n - \frac{f(x_n)}{f'(x_n)} \tag{C21}$$

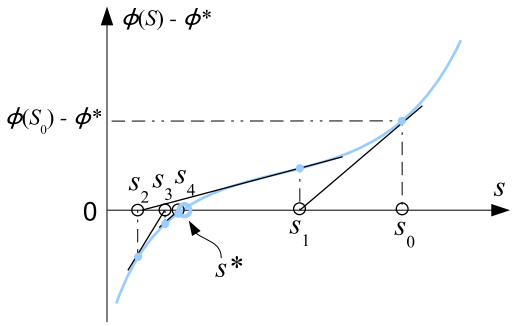

FIG. 23: Graph showing the progression of the Newton-Rhaphson method.

b. *Procedure for Newton-Raphson Method*

Since it is desired for ϕ to reach ϕ^*, we set $f(S) = \phi(S) - \phi^*$ such that $f(S^*) = 0$, where S^* is the value of S when $\phi = \phi^*$. We then have $f'(S) = \phi'(S) - 0$. Substituting into Eq (C21) gives

$$S_{n+1} = S_n - \frac{(\phi)_n - \phi^*}{(d\phi/dS)_n} \tag{C22}$$

Repeat until $(\phi)_n - \phi^* < \epsilon_{\phi^*}$.

c. *Limitations of Newton-Raphson Method*

4. Truncation Error in Numerical Solutions

Truncation error in the Runge-Kutta method contributes the greatest to the overall error in the numerical method, and thus other errors are neglected.

For the 4th-order Runge-Kutta method, the error is generally in the 5th order in the step length ΔS, which may be written as

$$\Delta E \approx k\Delta S^5 \tag{C23}$$

where k is some positive constant.

The error in $\Delta\phi$ is determined by first evaluating the change in ϕ, $\Delta\phi_1$ from ΔS, and then repeating the evaluation from the same point with two successive steps of $\Delta S/2$, to obtain $\Delta\phi_2$, as shown in Figure 24. The true change in ϕ for a step ΔS is

$$\Delta\phi = \Delta\phi_1 + \Delta E_1 = \Delta\phi_2 + \Delta E_2 \tag{C24}$$

where

$$\Delta E_1 \approx k\Delta S^5 \tag{C25a}$$
$$\Delta E_2 \approx 2k(\Delta S/2)^2 = k\Delta S^5/16 \tag{C25b}$$

since $\Delta E_{21} + \Delta E_{22}$ and $\Delta E_{21} = \Delta E_{22} \approx k(\Delta S/2)^5$.

Suppose a constraint for maximum error, $\Delta E_2 < \epsilon\Delta\phi$ ($\equiv \Delta E_1 < \epsilon'\Delta\phi$) is imposed. Then

$$\Delta E_2 < \epsilon\Delta\phi = \epsilon(\Delta\phi_2 + \Delta E_2) \tag{C26}$$

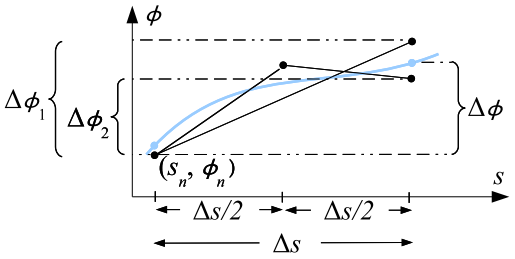

FIG. 24: Graph showing the error in $\Delta\phi$

which after rearranging gives

$$\Delta E_2 < \frac{\epsilon}{1-\epsilon}\Delta\phi_2 \approx \epsilon\Delta\phi_2 \tag{C27}$$

if $\epsilon << 1$. Rearranging Eq (C24) and substituting Eq (C25a) and (C25b) gives

$$\begin{aligned} \Delta\phi_2 + \Delta E_2 &= \Delta\phi_1 + \Delta E_1 \\ |\Delta\phi_2 - \Delta\phi_1| &= |\Delta E_1 - \Delta E_2| \\ &\leq |\Delta E_1| + |\Delta E_2| \\ &= 17\,|\Delta E_2| \\ &< 17\epsilon\,|\Delta\phi_2| \end{aligned} \tag{C28a}$$

When determining the values at critical angles, first apply the error constraint, then apply the Newton-Rhapson method to converge to the values.

Subject to the trunctation error requirement limit, ΔS is programmed to grow at 10% each step to keep it as large as possible (up to 2^o), for program efficiency.

5. Cubic Splines

A popular interpolation method, cubic splines, determine piece-wise cubic polynomials between every pair of points, with the added benefit of smooth continuity. So the functional value and first derivative at each point are equal also. More can be read in [15].

6. Fourier Cosine Series

We desire to have an easily reproducible expression for the shape of the raindrop, in polar coordinates with the center of mass of the drop as the origin. A Fourier series would be suitable for this, and since this function would be an even function due to the symmetry about the z-axis, the Fourier cosine series would be appropriate. From [16] we have

$$f(t) = \frac{a_0}{2} + \sum_{n=1}^{\infty} a_n \cos\frac{n\pi t}{L} \tag{C29}$$

where

$$a_n = \frac{2}{L}\int_0^L f(t)\cos\frac{n\pi t}{L} \tag{C30}$$

[1] K. V. Beard and C. Chuang, J. Atmos. Sci. **44**, 1509 (1987).
[2] C. Magono, J. Meteorol. **11**, 77 (1954).
[3] H. R. Pruppacher and R. L. Pitter, J. Atmos. Sci. **28**, 86 (1971).
[4] P. Savic, *Circulation and distortion of liquid drops falling through a viscous medium* (1953).
[5] A. Fage, Reports and memoranda - Aeronautical Research Committee **1766**, 20 (1937).
[6] W. F. Hughes and J. A. Brighton, *Schaums outline of theory and problems of fluid dynamics* (McGraw-Hill, 1991), chap. 5, pp. 75–92, 2nd ed.
[7] E. Achenbach, J. Fluid. Mech. **54**, 565 (1972).
[8] B. P. LeClair, A. E. Hamielec, and H. R. Pruppacher, J. Atmos. Sci. **27**, 308 (1970).
[9] W. F. Hughes and J. A. Brighton, *Schaums outline of theory and problems of fluid dynamics* (McGraw-Hill, 1991), chap. 6, pp. 106–135, 2nd ed.
[10] L. M. Milne-Thomson, *Theoretical Hydrodynamics* (St. Martins, 1960), chap. 15, pp. 452–492, 4th ed.
[11] D. R. L. et. al., ed., *CRC Handbook of Physics and Chemistry* (CRC Press, 2005), 86th ed.
[12] C. Isenberg, *The Science of Soap Films and Soap Bubbles* (Woodspring, 1978).
[13] S. Hartland and R. W. Hartley, *Axisymmetric Fluid-Liguid Interfaces* (Elsevier, 1976).
[14] M. Abramowitz and I. A. Stegun, *Handbook of Mathematical Functions with Formulas, Graphs, and Mathematical Tables* (Dover, 1972), chap. 21, p. 752, 10th ed.
[15] C. F. VanLoan, *Introduction to Scientific Computing* (Dover, 2000), chap. 3, 2nd ed.
[16] C. H. Edwards and D. E. Penney, *Differential Equations and Boundary Value Problems: Computing and Modeling* (Prentice-Hall, 2000), chap. 9.3, pp. 609–619, 2nd ed.
[17] Bad Rain Website `http://www.ems.psu.edu/\protect\protect\unhbox\voidb@x\penalty\@M\{}fraser/Bad/BadRain.html`
[18] Wikipedia entry on Runge-Kutta methods `http://en.wikipedia.org/wiki/Runge-kutta`